Engineering 56 (2026) 317–331

Contents lists available at ScienceDirect

Engineering

journal homepage: www.elsevier.com/locate/eng

Research
Agricultural Sensors—Review

An Analytical Comparison of the Performance of Various Sensing Materials and Mechanisms for Efficient Detection Capability of Greenhouse Gas Emissions

Mostafa Rastgou, Yong He, Qianjing Jiang *

Department of Biosystems Engineering, Zhejiang University, Hangzhou 310058, China

ARTICLE INFO

Article history:
Received 28 November 2023
Revised 28 October 2024
Accepted 13 November 2024
Available online 24 November 2024

Keywords:
Analytical comparison
Greenhouse gases
Sensing materials
Sensing mechanisms
Sensor

ABSTRACT

Increasing greenhouse gas (GHG) emissions, such as methane (CH_4), nitrous oxide (N_2O), and carbon dioxide (CO_2), from agricultural practices and land use have increased concerns about global warming. Accurate quantification of the GHG using gas sensors is essential for effective management and sustainable agricultural practices. The objective of this study was to make an analytical comparison of the performance of various sensing materials for CH_4-, N_2O-, and CO_2-based sensors in terms of sensitivity, response ratio, response time, and recovery time to establish an efficiency detection level of the GHG emissions. A literature review of 95 different studies showed that palladium–tin dioxide (Pd-SnO_2) nanoparticles, indium oxide (In_2O_3) nanowires, and gold-lanthanum oxide-doped tin dioxide (Au-La_2O_3/SnO_2) nanofibers had better performance compared to other sensing materials in CH_4-, N_2O-, and CO_2-based sensors, respectively. The findings from reviewed studies revealed that nanoporous structures, nanowires, and nanofibers had faster response and recovery compared to conventional materials due to their big specific surface area (SSA). The designed ternary hybrid structure of sensing materials was more effective for CO_2 gas detection than the double hybrid structure, unlike CH_4- and N_2O-based sensors. However, constructive suggestions for researchers were discussed in the conclusion based on the current research status and challenges to improve the performance of GHG sensors.

© 2024 THE AUTHORS. Published by Elsevier LTD on behalf of Chinese Academy of Engineering and Higher Education Press Limited Company. This is an open access article under the CC BY license (http://creativecommons.org/licenses/by/4.0/).

1. Introduction

1.1. The importance of greenhouse gas (GHG) emissions and its impact on the environment and health

The challenge of climate change in the Earth's environment due to an increase of GHG can significantly affect the environment, agriculture, food security, and human health. Natural disasters, loss of biodiversity, droughts, changes in rainfall patterns, ocean acidification, and escalating wildfires are other consequences of global warming and climate change caused by the increase in GHG. In other words, climate change is a threat to many aspects of the Earth's ecosystem, including human health, agriculture, water resources, forests, and wildlife, which can make all of them vulnerable and at risk. Carbon dioxide (CO_2), methane (CH_4), ozone (O_3), nitrous oxide (N_2O), sulphur hexafluoride (SF_6), hydrofluorocarbons (HFCs), nitrogen trifluoride (NF_3), perfluorocarbons (PFCs), and water vapor [1,2], which are known as GHGs, can be traced from various sources, including energy systems, industry, buildings, transportation, and agriculture [3]. Lamb et al. [3] presented global GHG emission trends of different sectors from 1990 to 2018. They reported that the largest share of GHG emissions in 2018 was attributed to the energy systems (34%), industry (24.5%), agriculture (21.2%), transport (14.3%), and building operations (6%) (Fig. 1). Although global GHG emissions are mainly composed of CO_2 (approximately 74%), other contributions are from CH_4, N_2O, and fluorinated gases, accounting for 17%, 5%, and 3% [4]. Human activities related to food systems, including agricultural practices and land use, have greatly raised GHG levels in the Earth's environment [5]. According to the report of the Intergovernmental Panel on Climate Change (IPCC), approximately 57% to 60% of total global N_2O emissions and around 43% to 50% of total global CH_4 emissions are attributed to agricultural practices. The emission of various GHGs in the agricultural systems greatly depends on the type of

* Corresponding author.
E-mail address: jqj713@zju.edu.cn (Q. Jiang).

https://doi.org/10.1016/j.eng.2024.11.008
2095-8099/© 2024 THE AUTHORS. Published by Elsevier LTD on behalf of Chinese Academy of Engineering and Higher Education Press Limited Company.
This is an open access article under the CC BY license (http://creativecommons.org/licenses/by/4.0/).

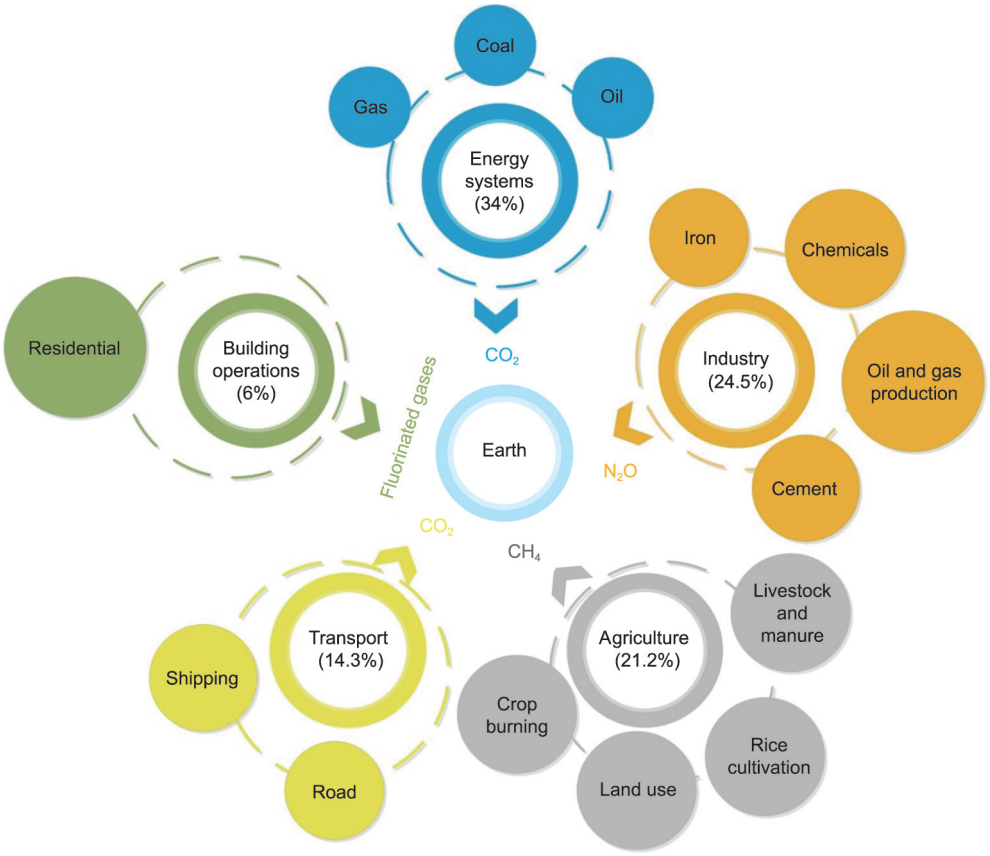

Fig. 1. Distribution of greenhouse gas emissions across various sectors according to the values reported by Lamb et al. [3].

agricultural practices and management. In particular, CH_4 is primarily emitted through enteric fermentation in ruminant livestock, such as cows, rice cultivation, and manure management [6]. Vaghar Seyedin et al. [7] made a comprehensive review of 159 studies and found that low livestock efficiency, poor-quality feed, lack of knowledge, and insufficient investment were the key factors contributing to methane gas emissions in low-income or developing countries. The N_2O emissions are mainly related to the management of agricultural soils, including the use of synthetic and organic fertilizers and the burning of crop residues [8]. In this regard, He et al. [9] made a global meta-analysis of 137 studies to assess the impact of organic fertilizers on GHG emissions compared to chemical fertilizers. Their findings revealed that N_2O emissions were significantly reduced by substituting organic fertilizers for chemical ones, while increasing global warming potential due to increased CH_4 and CO_2 emissions. Galic et al. [10] presented a review to evaluate the impact of agricultural management through fertilizers on CO_2, CH_4, and N_2O emissions. They reported that the use of organic modifiers has significant potential for protecting the environment and reducing GHG emissions. The CO_2 emissions from the agriculture sector can be released from various sources, including changes in land use, such as deforestation for agriculture, diesel fuel combustion in machinery, the burning of biomass for energy, and the use of synthetic fertilizers [11].

1.2. Importance of GHG sensors for improving food security in precision agriculture

The IPCC's fifth assessment report confirms that the overall GHG emissions continue to increase despite the implementation of various climate change mitigation policies. Learning about the challenge of climate change caused by GHG, the scientific community is diligently working to measure and quantify this phenomenon. The sensors have been designed to detect and measure the concentration of GHG in the atmosphere. These sensors generate valuable data by monitoring and providing real-time and accurate measurements of GHG emissions for assessing potential risks and challenges in food production systems [12]. This data-driven approach can be efficient in optimizing agricultural practices, enhancing productivity, and mitigating environmental impacts in the framework of food security and sustainable precision agriculture (Fig. 2) [13].

Numerous research groups globally have dedicated efforts to develop diverse sensor technologies for the detection of environmentally hazardous gases [14–16]. The technologies of GHG sensors are updated effectively and continuously through trial and error for more accurate measurements. Various manufacturing technologies have been developed for the detection of GHGs, such as catalytic gas sensors [17], optical gas sensors [18], metal oxide semiconductor-based sensors [17,19], electrochemical gas sensors [20], and nuclear sensors [16]. The performance of various sensors is determined by measurable parameters, including recovery and response time, detection limit, selectivity, operating temperature, response ratio, and sensitivity.

1.3. Unveiling the objectives

In recent decades, a large amount of research has focused on developing GHG sensors by creating new sensing materials, advancing manufacturing technologies, and enhancing sensor performance [16,19,21]. In the present study, the technical performance of various sensing materials and mechanisms in the GHG sensors is investigated based on quantitatively different parameters, including sensitivity, response ratio, response time, and recovery time. This study can provide a roadmap for more efficient selection of sensors in controlling GHG emissions.

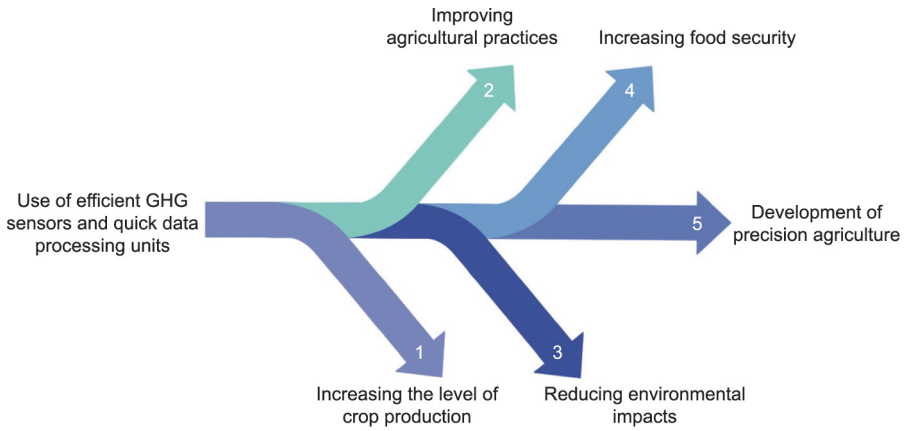

Fig. 2. Advantages of utilizing efficient sensors for detecting GUGs gases in the development of precision agriculture.

Therefore, the strategies and objectives of the present study can be listed as follows: ① providing an analytical comparison of the performance of GHG sensors in terms of sensing materials and mechanisms, ② identifying the ambiguities, limitations, and gaps in existing sensor technologies, and ③ providing constructive suggestions based on the current research status and identified challenges to improve the accuracy and efficiency of GHG sensors.

2. Methods

The GHG sensors are classified by the sensing mechanism [14] and sensing material [17], which are discussed separately in the following subsections.

2.1. Classification of GHG sensors by sensing mechanism

2.1.1. Resistance measurement (RM) sensor

Resistance-based sensors are devices that measure the concentration of GHG by monitoring changes in electrical resistance [14]. The schematic mechanism of a resistance-based sensor is illustrated in Fig. 3(a). This sensor responds to GHG through a sensing element, which is often composed of or coated with various active materials such as metal oxide semiconductors or carbon nanomaterials. These elements are connected to a circuit, which measures the resistance of the sensing material [22]. This resistance changes when the sensing material interacts with the target gas, due to the adsorption of gas molecules onto the element's surface. Consequently, the type and quantity of gas could lead to either an increase or decrease of the electrical resistance of the sensing material [23]. Finally, the electrical resistance of sensing material can be interpreted as the concentration of the GHG by comparing the resistance value to a calibration curve or mathematical equation of the target gas.

2.1.2. Field effect transistor (FET) sensor

The schematic mechanism of the FET-based sensor is depicted in Fig. 3(b). The basic structure of a typical FET-based gas sensor consists of four parts, including source and drain electrodes, a sensing layer or conductive channel, a gate electrode, and an insulator. In these sensors, the conductive channel is in contact with target gas on the gate electrode. Materials such as graphene, carbon nanotubes, or metal oxides are commonly used in the conductive channel [24,25]. When the sensor encounters target gas, gas molecules are adsorbed onto the surface of the channel material. This adsorption process leads to a charge transfer between gas molecules and the channel. The change in the channel conductivity is measured as a change in current between the source and drain electrodes [26]. By analyzing these changes in the FET's current and voltage, the concentration of GHG in the environment can be quantified using calibration curves or mathematical models.

2.1.3. Surface acoustic wave (SAW)-based micromechanical sensor

The SAW-based sensor uses surface acoustic wave technology to propagate acoustic waves along the surface of a solid material, such as quartz. The schematic mechanism of the SAW-based sensor is illustrated in Fig. 3(c). In these sensors, a piezoelectric substrate, such as quartz or lithium niobate, generates a surface acoustic wave that propagates along its surface. A gas-sensitive material is deposited on the SAW propagation path. This layer can be metal oxide, polymer, or other material that interacts with the target gas. When the sensor encounters the target gas, gas molecules are adsorbed onto the sensitive layer. The adsorbed gas molecules increase the mass of the sensitive layer, altering the SAW velocity. This change in SAW velocity is directly related to the mass of the adsorbed gas, which can be quantified through Fourier analysis, wavelet analysis, or statistical modeling [27,28].

2.1.4. Electrochemical sensor

Electrochemical-based sensors are devices that measure the concentration of GHG in the atmosphere based on the principle of redox reactions. Fig. 4(a) shows the schematic mechanism of the electrochemical sensor. An electrochemical sensor typically consists of working (sensing) electrode, counter electrode, and reference electrode, which are separated by the electrolyte to have the electrochemical reaction with the target gas. The absorbed gas molecules onto the surface of the working electrode generate an electric current at the sensing electrode through an electrochemical reaction. This electric current is directly proportional to the concentration of the target gas. Then, the sensor converts this electric current into a readable output, such as a voltage or a digital signal, which can be used to determine the gas concentration [13,20]. It is important to note that the FET-based sensors are not classified as electrochemical sensors. The FET-based sensors utilize the electrical field generated by the charges on the gate electrode to detect changes in the concentration of the target gas. In contrast, electrochemical sensors rely on chemical reactions to produce an electrical signal through the oxidation or reduction of analytes in a solution.

Catalytic gas sensors operate based on the principle of heat production resulting from the catalytic combustion of specific gases [29]. Fig. 4(b) illustrates the schematic mechanism of catalytic sensors. The sensor's core component is a catalytic material, which is highly effective in oxidizing combustible gases. The vast majority of metal oxides including tin dioxide (SnO_2) and tungsten trioxide

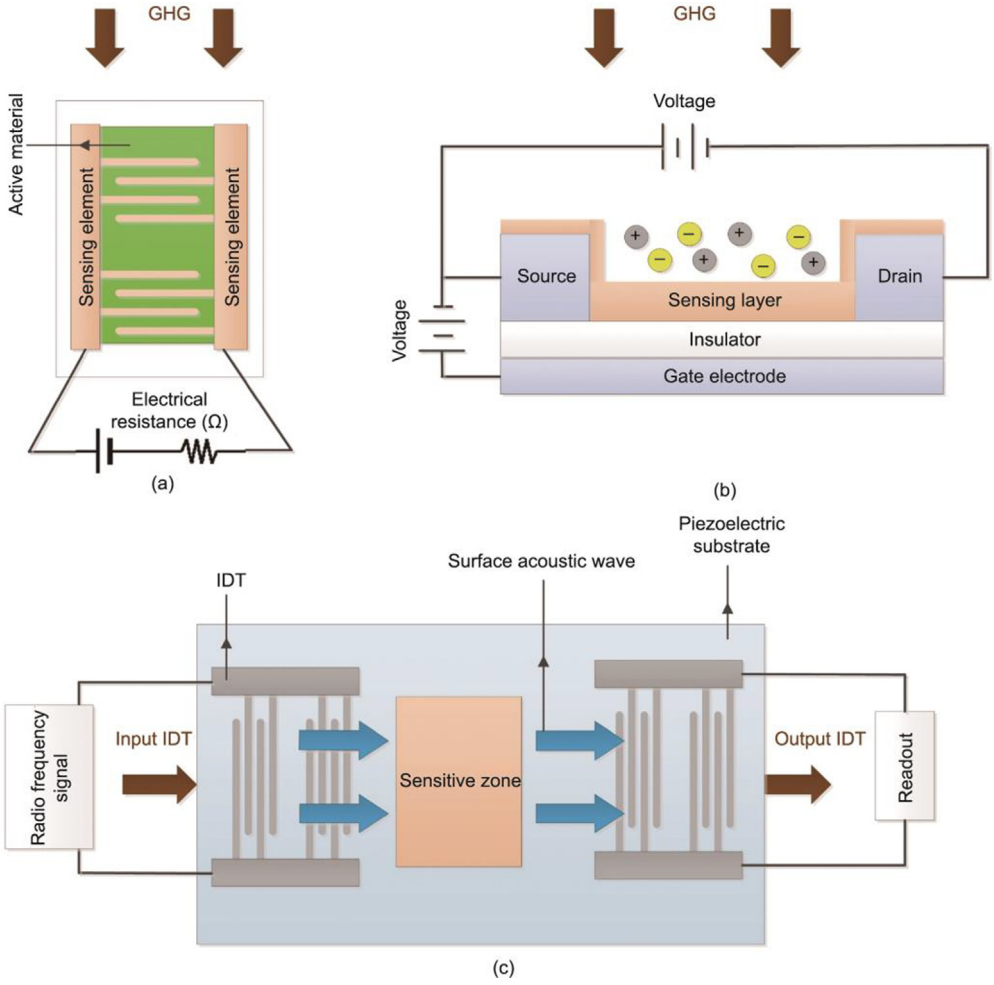

Fig. 3. Schematic mechanisms of GHG sensors based on (a) resistance measurement, (b) field effect transistor, and (c) surface acoustic wave. IDT: interdigital transducer.

(WO_3), as well as noble metals such as platinum (Pt) and palladium (Pd) have catalytic behaviors. The heat produced raises the temperature of the catalytic element. The temperature change affects the electrical resistance of a heating element located near the catalytic material. This change in resistance is measured and converted into an electrical signal that corresponds to the gas concentration [30].

2.1.5. Gas chromatography (GC) technique

The GC technique operates on the principle of separating different gases based on their distinct chemical characteristics [16,31,32]. Fig. 5(a) shows the schematic mechanism of the GC technique. The GC technique comprises the sample injector, separation column, detector, and data acquisition system. In the sample injector component, the GHG is introduced into the system. Then, the gas mixture is transported through a separation column, which contains a stationary phase that selectively interacts with different compounds. As the gases cross the column, they are separated based on their affinity for the stationary phase. Each gas is identified by a detector, such as a thermal conductivity detector or a flame ionization detector. The detector produces a signal proportional to the concentration of each gas, which is recorded by the data acquisition system. This data can be used to quantify the amount of specific GHG present in the sample.

2.1.6. Optical sensor

The optical gas sensor uses optical technology to detect and quantify the concentration of GHG in the atmosphere. In other words, these sensors can measure the amount of light absorption by the GHG in different wavelengths. The schematic mechanism of the optical gas sensor is illustrated in Fig. 5(b). Typically, the optical gas sensor consists of a light source, such as an light emitting diode (LED) or laser, and a detector [33]. The light passes through a sample of gases, and the detector measures the amount of light absorbed by the gases present. These sensors can determine the concentration of GHG using distinct absorption spectra. Different types of optical gas sensors, including laser absorption spectroscopy (LAS) [34], nondispersive infrared (NDIR) [35], and photoacoustic spectroscopy (PAS) [36], use optical principles to detect and measure the concentration of GHG. Generally, the main differences between these optical gas sensors are their detection principles and signal extraction methods. The LAS sensor uses a laser beam to illuminate gas samples, while the GHG absorbs light with specific wavelengths based on their molecular composition. The NDIR sensors use an infrared light source and a detector that measures the amount of infrared light absorbed by the gases in the sample. The PAS technique uses laser-induced acoustic waves to detect and analyze gases. These waves are captured by a microphone or other acoustic detection methods and can be interpreted as the concentration of GHG.

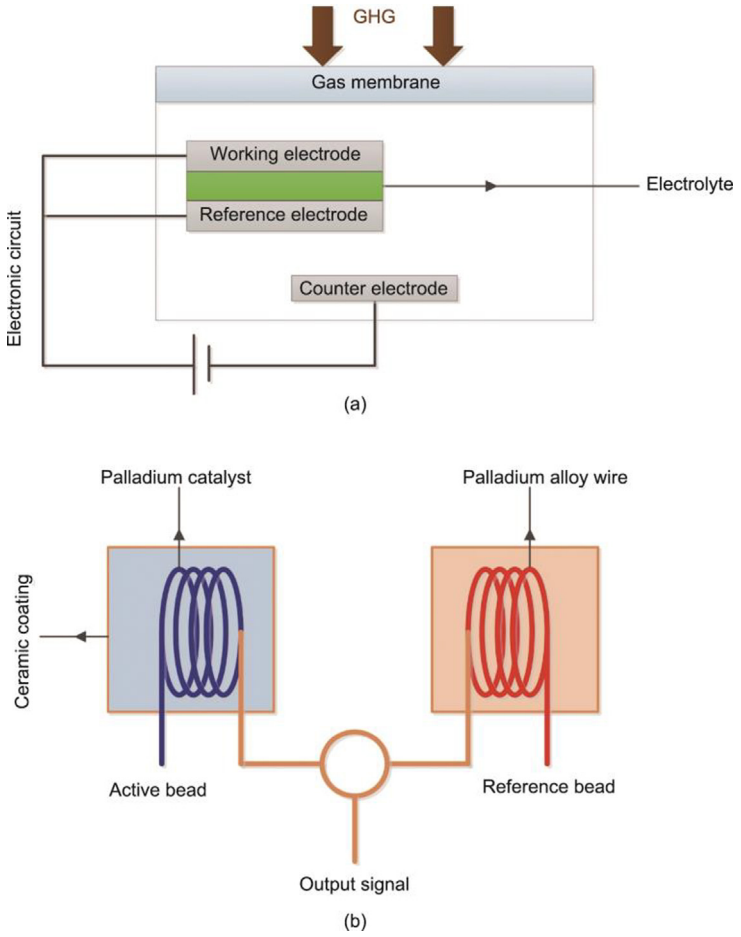

Fig. 4. Schematic mechanisms of GHG sensors based on (a) electrochemistry and (b) catalyst.

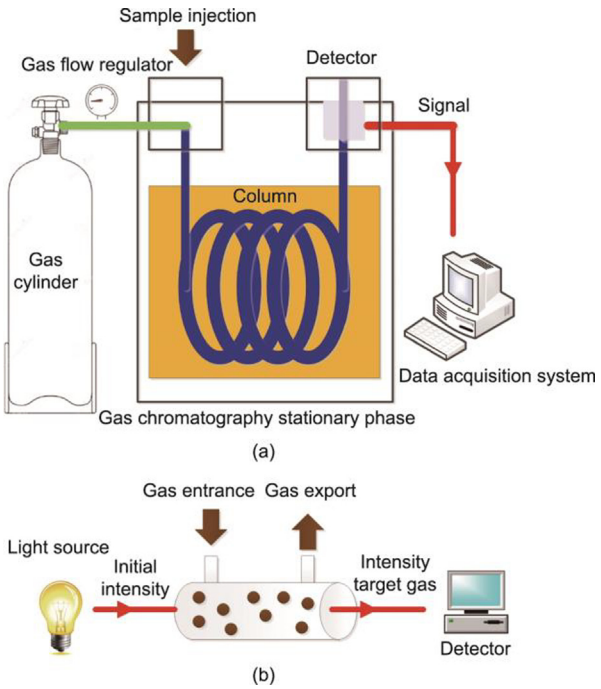

Fig. 5. Schematic mechanisms of GHG sensors based on (a) chromatography and (b) optics.

2.2. Detection of GHG emissions based on sensing materials in different sensors

In the last few years, a range of sensing materials for various sensors have been developed for the detection of GHG [37]. Some of these materials are costly and involve complex synthesis processes, which can hinder research and large-scale application [38]. Metal oxides (e.g., SnO_2, zinc oxide (ZnO), WO_3, cerium oxide (CeO_2), indium oxide (In_2O_3), and titanium dioxide (TiO_2)) and metal catalysts (e.g., Pt, Pd, and rhodium (Rh)) are known as the most important sensing materials in various sensors for detecting GHG (Fig. 6). Different types of nanomaterials, including nanoparticles and nanowires composed of sensing materials such as metal oxides, carbon nanotubes, and graphene, have demonstrated significant potential for gas sensing applications. Conductive polymers, such as polyaniline (PANI), polythiophene (PT), and polypyrrole (PPy), have become highly promising materials for the development of gas sensors. These conductive polymeric materials are often used in gas sensors because of their electrical and chemical properties, which include high sensitivity, selectivity, cost effectiveness, ease of fabrication, and mechanical resilience [39,40]. In contrast to many traditional gas sensors that require high operating temperatures, sensors based on conductive polymers can work effectively at room temperature, which reduces energy consumption [41]. The great conductivity of these materials makes rapid and sensitive detection of gas molecules possible. Additionally, PANI and PPy are very suitable for long-term monitoring of GHG emissions due to their high stability and durability. In other words, these materials can endure harsh environmental

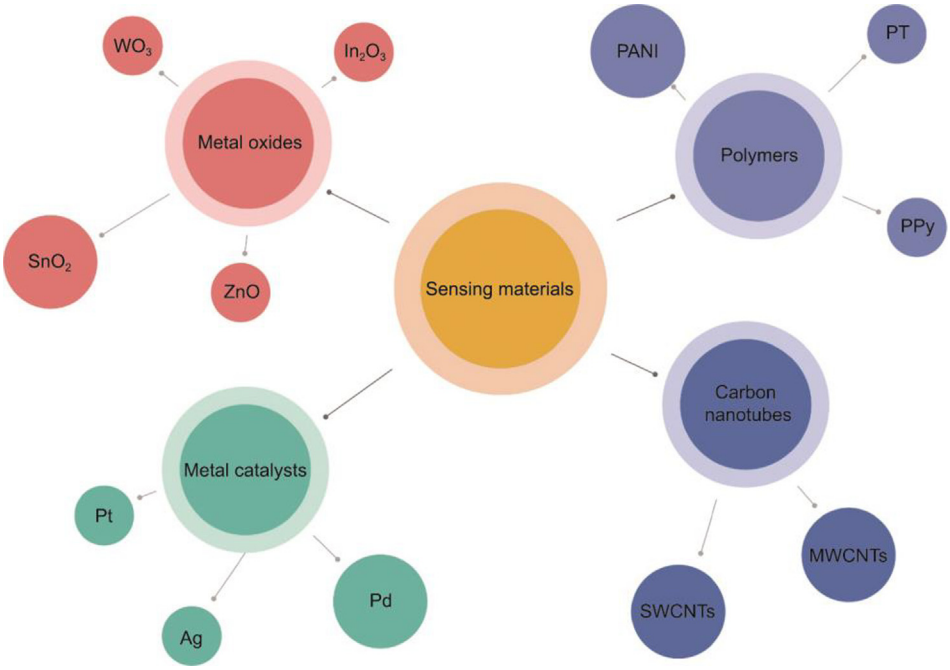

Fig. 6. Classification of sensing material types in sensors for detecting greenhouse gases. Ag: silver; PANI: polyaniline; PT: polythiophene; PPy: polypyrrole; SWCNTs: single-walled carbon nanotubes; MWCNTs: multi-walled carbon nanotubes.

conditions and continuous exposure to gases without degradation, ensuring reliable and consistent performance over an extended period. It is important to note that the selection of sensing material depends on the target gas for detection, because different sensing materials have different degrees of sensitivity and selectivity for different gases.

2.3. Criteria for evaluating the performance of GHG sensors

Sensor performance refers to the accuracy, sensitivity, and reliability of the sensor in detecting and measuring GHG. Properties of sensing material, including response time, recovery time, sensitivity, and response ratio, can be used to investigate and evaluate the performance of GHG sensors [19,23]. The sensitivity refers to the ability of the sensor to detect and measure the change in response per unit change in gas concentration [42]. A sensor with high sensitivity can accurately detect even GHG with low concentrations as the lowest limit. Furthermore, the sensitivity of a sensor can also affect its ability to detect and distinguish different GHG, as well as its response time and reliability. The response ratio can be defined as $(|R_2 - R_1|)/R_1$, where R_1 and R_2 are the sensor responses at the lower and higher gas concentrations, respectively [43]. A high response rate indicates that the sensor detects changes in gas concentrations quickly. Response time refers to the duration it takes for the sensor to accurately and meaningfully measure after detecting target gas. A shorter response time is crucial for real-time monitoring applications, where immediate and accurate readings are required. On the other hand, the recovery time refers to the duration it takes for the sensor to return to its initial state after detecting and measuring the GHG. This is particularly important to ensure that subsequent readings are not affected by residual gases or contaminants. A high-performance GHG sensor with shorter recovery and response time can provide accurate and near-real-time measurements to effectively control emissions. Taking these points into account, in the present study, the performance of GHG sensors is evaluated based on response time, recovery time, sensitivity, and response ratio on sensing materials and mechanisms in 95 different studies in the last two decades, including 42 studies related to CH_4 gas, 14 studies related to N_2O gas, and 39 studies for CO_2 gas. Consequently, studies in which these parameters were not reported were excluded from this review. The literature review revealed that many researchers have concentrated on the reactivity of various sensing materials with the target gas, while paying less attention to the mechanisms of the sensors. In contrast to the extensive research dedicated to enhancing the sensing material properties of CH_4- and CO_2-based sensors, relatively few studies have focused on the improvement of N_2O-based sensors in this regard.

3. Results and discussion

3.1. Performance evaluation of different sensing materials in CH_4-based sensors

A comparison of the performance of different sensing materials based on response time, recovery time, sensitivity, and response ratio in CH_4-based sensors is summarized in Table 1 [42–83]. According to the studies by Abruzzi et al. [43] and Yao et al. [44] presented in Table 1, Pd-doped SnO_2 nanoparticles utilizing the resistance change technique had the best performance in terms of response time (3 s), recovery time (5 s), sensitivity (S = 83%), and response ratio (R = 17.6) compared to other sensing materials in CH_4-based sensors. The good performance of Pd-doped SnO_2 nanoparticles as a sensing material in CH_4-based sensors can be attributed to the effective combination of several reasons, including sensitivity, specific surface area (SSA) or surface chemistry, and catalytic activity and stability. Pd-doped SnO_2 nanoparticles can enhance the SSA and oxygen species while altering the morphology of the sensing material to facilitate CH_4 oxidation. This increased SSA provides more active sites for gas adsorption and promotes the chemisorption of CH_4 molecules, which can improve the sensitivity and response ratio of the CH_4 gas sensor. In other

Table 1
A comparison of the performance of different sensing materials based on response time, recovery time, response ratio, and sensitivity in CH_4-based sensors.

Study	Sensing material and structure	Formula	Response time (s)	Recovery time (s)	Response ratio (R) or sensitivity (S)
Ref. [49]	Tin dioxide thin film	SnO_2	—	—	R = 14.5
Ref. [50]	Palladium in tin dioxide nanoporous	Pd-SnO_2	—	—	R = 10–20
Ref. [51]	Graphene nanosheets/polyaniline nanocomposite	—	85	45	S = 5%
Ref. [52]	Platinum-functionalized nickel oxide nanotubes	NiO-Pt	—	—	R = 1.02
Ref. [53]	Vanadium dioxide nanostructured films	VO_2	—	—	S = 3.2%
Ref. [54]	Nickel oxide-decorated tin dioxide particulate films	Ni_2O_3/SnO_2	—	—	R = 1.27
Ref. [55]	Platinum electrode with ionic liquid electrolyte	—	13	—	S = 22.7 $\mu A \cdot cm^{-2} \cdot \%^{-1}$
Ref. [56]	Tin dioxide nanorods	SnO_2	13	—	S = 20.9%
Ref. [57]	Silver–tin dioxide composite	Ag–SnO_2	—	—	S = 75%
Ref. [58]	Polycarbonate/cryptophane	—	5	—	S = 2.5 $nm \cdot \%^{-1}$
Ref. [59]	Vanadium dioxide nanorods	VO_2	75	158	S = 15%
Ref. [48]	Gold-decorated vanadium dioxide nanosheets	Au/VO_2	—	—	S = 70%
Ref. [60]	Gold-decorated vanadium oxide films	Au/VO_x	—	—	S = 25%
Ref. [61]	Platinum nanoparticles-decorated vanadium oxide films	Pt/VO_x	—	—	S = 18.2%
Ref. [62]	Cadmium titanate films	$CdTiO_3$	38	70	S = 3.4 %
Ref. [63]	Vanadium pentoxide films	V_2O_5	—	—	R= 0.28
Ref. [64]	Cobalt oxide nanoparticles	Co_3O_4	100	50	R = 1.28
Ref. [65]	Platinum electrode with ionic liquid electrolyte	—	—	—	S = 0.3 $\mu A \cdot cm^{-2} \cdot \%^{-1}$
Ref. [66]	Tin-doped indium oxide and platinum electrodes	Sn-ITO/YSZ	15	—	R = 44 $mV \cdot 100\ ppm^{-1}$
Ref. [67]	Palladium-doped tin dioxide nanosize	Pd/SnO_2	6	10	R = 12.4
Ref. [68]	Platinum-containing tin dioxide nanosize	Pt-SnO_2	7	16	S = 14.5
Ref. [46]	Palladium-doped tin dioxide -reduced graphene oxide	Pd-SnO_2/rGO	300	420	S = 9.5%
Ref. [69]	Vanadium oxide-walled carbon nanotubes	VO_x	16	120	S = 1.5%
Ref. [42]	Iron borate nanocrystalline	Fe_3BO_6	60	96	S = 43%
Ref. [70]	Palladium-loaded Tin dioxide hollow spheres	Pd-SnO_2	3	7	R = 4.88
Ref. [71]	Cobalt-doped zinc oxide nanoparticles	Co-ZnO	25.2	6.6	R = 1.05
Ref. [72]	Platinum-loaded tin dioxide nanofibers	Pt-SnO_2	24.3	141.1	R = 4.48
Ref. [73]	Polyaniline/multi-walled carbon nanotubes/molybdenum disulfide	PANI/MWCNTs/MoS_2	—	—	R = 2.5
Ref. [45]	Tin dioxide nanorods-graphene hybrids	SnO_2	369	519.8	S = 24.9%
Ref. [74]	Solid polymer electrolyte-infused laser induced graphene	—	40	—	S = 0.55 $\mu A \cdot ppm^{-1} \cdot cm^{-2}$
Ref. [75]	Tin dioxide-decorated nickel oxide nanaosheets	SnO_2/NiO	28	44	S = 15.2%
Ref. [76]	Tin dioxide nanoporous	SnO_2	1	3	R = 9.8
Ref. [43]	Palladium-doped tin dioxide nanoparticles	Pd/SnO_2	16	70	S = 83%
Ref. [77]	Platinum nanoparticles-doped tin dioxide nanoflowers	Pt/SnO_2	1.5	100	R = 1.98
Ref. [78]	Complex metal oxide electrode	$SmMn_2O_5$	27	33	R = −44.5 $mV \cdot decade^{-1}$
Ref. [79]	Zinc Stannate-decorated zinc oxide microflower	Zn_2SnO_4/ZnO	10	30	R = 15.36
Ref. [80]	Vanadium pentoxide nanoflowers	V_2O_5	206	247	S = 8%
Ref. [47]	Oxygen vacancy-enriched zinc oxide/palladium nanorods	OV ZnO/Pd	420	300	S = 36.8%
Ref. [44]	Palladium-tin dioxide composite	Pd-SnO_2	3	5	R = 17.6
Ref. [81]	Tin dioxide-graphene nanomaterial	SnO_2/Graphene	—	—	S = 12.2%
Ref. [82]	Gold-tin dioxide	Au-SnO_2	—	—	R = 1.2
Ref. [83]	Non-dispersive infrared (NDIR) gas sensor	—	140	157	R = 3.1

In these sensors, the unit can be represented as a ratio or percentage. In electrochemical-based sensors, the response or sensitivity is generally expressed in terms of the change in signal (often current or voltage) per unit concentration of the gas.

words, incorporating Pd nanoparticles into SnO_2 increases the sensitivity in the absorption and oxidation reactions between CH_4 and SnO_2 due to the high affinity of Pd for CH_4 gas molecules. This can lead to improved performance of sensing material in response and detection of CH_4 gas. Yao et al. [44] indicated that the nanoporous structure of Pd-SnO_2 and chemical sensitization of Pd could be considered as an effective strategy for achieving exceptional gas sensing performance in CH_4-based sensors.

It should be noted that high SSA is a necessary but not sufficient condition for the performance of sensing materials. The SnO_2 nanorods–nanoporous graphene in the study of Kooti et al. [45] had a higher SSA than Pd-SnO_2 in the study of Abruzzi et al. [43] (162.09 $m^2 \cdot g^{-1}$ vs 50 $m^2 \cdot g^{-1}$), but lower sensitivity was observed in the detection of CH_4 gas by SnO_2 nanorods–nanoporous graphene (24.9% vs 83%). Therefore, it appears that a variety of other factors such as the catalytic effect can significantly affect the performance of the sensing materials. Due to their high catalytic activity, Pd nanoparticles enhance the reaction kinetics of CH_4 oxidation on the surface of the sensing material, facilitating the conversion of CH_4 to CO_2 and H_2O. This catalytic activity, acting as a form of chemical sensitization, decreases the operating temperature required for CH_4 gas detection, making it a highly effective sensing material for CH_4-based sensors [43]. Similar findings were also reported by Nasresfahani et al. [46]. Pd-doped SnO_2 nanoparticles prevents degradation of sensing material and increases the stability, durability, reproducibility, and reliability of the sensor against environmental factors and multiple sensing cycles over an extended period.

Sensing materials of Pd nanoparticles-doped ZnO nanorods [47], SnO_2 nanorods–graphene nanoporous hybrid [45], and Pd-decorated ZnO/reduced graphene oxide hybrid [46] had the longest sensing response time of 420, 369, and 300 s, respectively (Table 1). It seems that there is still a long way to go to design CH_4 gas sensors based on ternary hybrids. A crucial aspect to consider in ternary hybrid-based sensors is the synergistic effect of the sensing materials, ensuring that the combined effect of all three components is greater and more effective than that of each individual component. Pd-doped SnO_2 nanoporous sensor had a shorter response and recovery time than Pd-doped ZnO nanorods sensor (Table 1). This could be attributed to the optimized structure and composition of the SnO_2 nanoporous material, which increases the interaction between CH_4 and the surface of the sensing material. Gold (Au) nanoparticles-decorated vanadium dioxide (VO_2) nanosheets sensor had a high sensitivity of 45% at room

temperature for 100 ppm of CH_4 compared to other sensing materials, which could be attributed to the formation of a heterojunction at the interface of the VO_2 nanosheets and Au nanoparticles [48]. Additionally, the Au nanoparticles-decorated VO_2 nanosheets sensor had higher sensitivity than VO_2 nanorods (45% vs 15%), which could be caused by the catalytic effect of Au.

The research findings from various literature studies on CH_4-based sensors (Table 1) revealed that certain nanostructure morphologies, such as nanoporous, nanorods, and nanosheets, had higher sensitivity and response ratio compared to those of conventional materials with larger SSA. Additionally, Pd nanoparticles, which have a more effective catalytic effect in sensing materials, improve the response ratio and performance of the CH_4-based sensors.

3.2. Performance evaluation of different sensing materials in N_2O-based sensors

In N_2O-based sensors, Table 2 [49,84,85,89–99] pointed to the fact that WO_3 nanowires with a diameter ranging from 0.5 to 15 nm had the best performance in terms of response time (10 s), recovery time (60 s), and sensitivity (S = 2690% to 100 ppm) compared to other sensing materials using the resistance change and electrochemical techniques, as noted in the studies by Deb et al. [84] and Rout et al. [85]. Additionally, Rout et al. [85] reported a high response ratio (R = 40 to 60) for In_2O_3 nanowires with a diameter of 20 nm in the detection of N_2O gas (Table 2).

The good performance of WO_3 and In_2O_3 nanowires makes them ideal sensing materials for N_2O gas sensors, attributed to several factors, including high surface-to-volume ratio, morphology and stability against humidity and temperature. Single crystalline nanowires and nanowire networks (mats) serve as efficient devices with an exceptionally high surface-to-volume ratio, showing great potential for detecting N_2O gas at low concentrations [86]. Nanowires have a high surface-to-volume ratio, which provides numerous active surface sites for N_2O gas molecules to interact with the sensing material. This increases the sensitivity and response ratio of the sensor to N_2O gas. In this regard, various studies have demonstrated that WO_3 nanowires have high sensitivity to nitrogen oxide (NO_x) gases, including N_2O, and can accurately detect and measure N_2O gas at very low concentrations [85–88].

The morphology and one-dimensional structure of nanowires can increase gas diffusion and absorption. These characteristics can improve gas absorption and sensor response time by providing a pathway for gas molecules to easily access active surface sites. In other words, the presence of oxygen vacancies and/or other defects in the structure of WO_3 and In_2O_3 nanowires can create and facilitate surface states or trap states for gas absorption, thereby increasing the conductivity changes induced by gas molecules. In relation to the structure of the nanowires, Deb et al. [84] reported that highly networked nanowires had higher sensitivity in detecting N_2O gas when used as sensing materials compared to randomly oriented nanoparticle layers. On the other hand, the WO_3 nanowires have rapid response and recovery, facilitating real-time monitoring of N_2O levels in the atmosphere. The WO_3 nanowires have high stability and durability against increasing thermal conditions and relative humidity, allowing them to withstand the elevated operating temperatures typically necessary for gas sensing applications. Such stability ensures the longevity of the sensors over extended periods under harsh conditions, such as high temperatures and varying humidity levels, without significant performance degradation.

The research findings of several literature studies on N_2O-based sensors (Table 2) revealed that nanowires and networked nanowires had higher sensitivity and response ratios compared to conventional materials with larger SSA. Besides, WO_3 and In_2O_3 nanowires, known for their high sensitivity and response ratios respectively, can be used in CH_4-based sensors, while the WO_3 nanowires provide a better response time.

3.3. Performance evaluation of different sensing materials in CO_2-based sensors

In CO_2-based sensors, the results in Table 3 [82,100–137] showed that barium titanate ($BaTiO_3$)–CuO–Ag with nanocomposite structures and 400 nm nanofilms had the best performance based on response time (3 s), recovery time (5 s), and sensitivity (S = 27%) compared to other sensing materials utilizing the resistance change technique, as reported by Joshi et al. [100] and Herrán et al. [101]. The good performance of $BaTiO_3$–CuO–Ag nanostructures as a sensing material in CO_2 gas sensors can be attributed to several key factors, including a big surface area,

Table 2
A comparison of the performance of different sensing materials based on response time, recovery time, response ratio, and sensitivity in N_2O-based sensors.

Study	Sensing material and structure	Formula	Response time (s)	Recovery time (s)	Response ratio (R) or sensitivity (S)
Ref. [89]	Tin dioxide thin film	SnO_2	—	—	R = 0.58
Ref. [90]	Samarium oxide-doped tin dioxide electrode	Sm_2O_3–SnO_2	90	180	S = 45 mV
Ref. [91]	Cadmium oxide powder	CdO	—	—	R = 1.03
	Indium oxide powder	In_2O_3	—	—	R = 1.05
	Tin dioxide powder	SnO_2	—	—	R = 1.66
	Zinc oxide powder	ZnO	—	—	R = 1.21
	Tungsten oxide powder	WO_3	—	—	R = 1.32
	Strontium oxide-loaded tin dioxide powder	SrO-SnO_2	20	60	R = 4.3
Ref. [49]	Gold-doped tin dioxide thin film	Au/SnO_2	—	—	R = 11.5
Ref. [85]	Indium oxide nanowires	In_2O_3	20	20	R = 60
	Tungsten oxide nanowires	WO_3	10	60	R = 25
Ref. [84]	Tungsten oxide nanowire	WO_3	354	1080	S = 2690%
Ref. [92]	Spinel magnesium zinc ferrite powders	$Mg_{0.5}Zn_{0.5}Fe_2O_4$	83.76	83.80	S = 19%
Ref. [93]	Silicon with wire width ranging from 233 to 340 nm	—	< 60	< 60	S = 21.4%
Ref. [94]	Yttria-stabilized zirconia (YSZ) electrolyte	—	20	60	R = 0.35 mA·%$^{-1}$
Ref. [95]	Aqueous alkaline ascorbate and diphenylphosphine/propylene carbonate electrolytes	—	—	—	S = 0.05 pA·nmol^{-1}
Ref. [96]	Tetracyanonickelate/KOH/reduced graphene oxide fabricated carbon felt	TCN(II)–KOH-rGO/CF	—	—	R = −36.5 μA·cm^{-2}·ppm^{-1}
Ref. [97]	Nickel phthalocyanine tetrasulfonic acid tetrasodium salt	Ni(I)TSPc	500	—	S = −0.012 mA·ppm^{-1}·cm^{-2}
Ref. [98]	Gold nanoparticles-decorated molybdenum disulfide	MoS_2-Au	406	516	R = 15.8
Ref. [99]	Copper oxide/titanium dioxide nanorods	CuO/TiO_2	36	50	R = 0.011

Table 3
A comparison of the performance of different sensing materials based on response time, recovery time, response ratio, and sensitivity in CO_2-based sensors.

Study	Sensing material and structure	Formula	Response time (s)	Recovery time (s)	Response ratio (R) or sensitivity (S)
Ref. [107]	Lanthanum oxide-doped tin dioxide film	La_2O_3-SnO_2	—	—	R = 1.4
Ref. [108]	Lanthanum oxychloride-doped tin dioxide powder	LaOCl-SnO_2	—	—	R = 1.6
Ref. [109]	Indium sesquitelluride thin film	In_2Te_3	—	—	R = 1.1
Ref. [110]	Complex carbonate electrode	Li_2CO_3–$BaCO_3$	15	20	S = 60.7 mV·decade^{-1}
Ref. [111]	Barium titanate–copper oxide thin film	$BaTiO_3$–CuO	120	78	S = 18%
Ref. [101]	Barium titanate–copper oxide–silver thin film	$BaTiO_3$–CuO–Ag	900	600	S = 27%
Ref. [112]	Barium titanate–copper oxide thin film	$BaTiO_3$–CuO	300	300	R = 3.3
Ref. [113]	lanthanum oxide-doped tin dioxide film	La_2O_3/SnO_2	—	—	R = 1.52
Ref. [105]	Lanthanum oxychloride-doped tin dioxide film	LaOCl-SnO_2	15	19	R = 5.6
Ref. [114]	Sodium-ion conducting electrolyte and complex carbonate electrode	Na_2CO_3–$CaCO_3$	< 12	—	S = 66 mV·decade^{-1}
Ref. [115]	Indium telluride thin film	In_2Te_3	15-20	—	R = 1.1
Ref. [116]	Lanthanum oxychloride-doped zinc oxide nanowires	LaOCl/ZnO	15	17	R = 4
Ref. [117]	Lithium-based electrode and electrolyte	$Li_6BaLa_2Ta_2O_{12}$-$Li_{0.36}WO_3$	—	—	S = 73 mV·decade^{-1}
Ref. [118]	Perovskite oxides nanocrystalline powders	$LaFeO_3$	240	480	R = 2.19
Ref. [119]	Zinc oxide thin film	ZnO	20	20	S = 1.13%
Ref. [120]	Lanthanum-doped tin dioxide thick film	La-SnO_2	20	75	R = 1.4
Ref. [121]	Zinc oxide nanowires	ZnO	8	40	S = 3.8%
Ref. [122]	Calcium-doped zinc oxide nanopowders	Ca/ZnO	—	—	R = 1.1
Ref. [106]	Tin-doped cadmium oxide nanostructure	Sn/CdO	275	150	S = 15%
Ref. [123]	Titanium dioxide/aluminium oxide heterostructure	TiO_2/Al_2O_3	—	—	R = 1.4
Ref. [124]	Chromium-doped titanium dioxide thin films	Cr/TiO_2	81	63	R = 1.8
Ref. [125]	Platinum-lanthanum oxide-doped tin dioxide film	Pt/La_2O_3/SnO_2	—	—	R = 4.38
Ref. [126]	Nanostructured copper oxide	CuO	10	6	S = 3.5%
Ref. [127]	Perovskite $LaFeO_3$/tin dioxide thick film	$LaFeO_3$/SnO_2	18	—	R = 2.7
Ref. [128]	Silver–copper(II) oxide/zinc oxide nanoleaves	Ag–CuO/ZnO	76	265	R = 0.35
Ref. [129]	Palladium-nanoparticle decorated polyaniline films	Pd-PANI	—	—	R = 1.7
Ref. [100]	Silver-copper(II) oxide/barium titanate nanocomposite	Ag-CuO/$BaTiO_3$	3	5	R = 1.4
Ref. [103]	Barium-doped cobalt oxide powder	Ba-Co_3O_4	192	215	S = 5%
Ref. [104]	Lanthanum oxide-doped tin dioxide stacked layers	La_2O_3/SnO_2	—	—	R = 2.9
Ref. [130]	Lithium-based electrode and electrolyte	Li_3PO_4-Li_2CO_3	60	—	S = 50.5 mV·decade^{-1}
Ref. [131]	Copper oxide nanoparticles-zinc peroxide	CuO-ZnO_2	—	—	R = 1.3
Ref. [132]	Lithium-ion electrolyte	Li_3PO_4-Li_2SiO_3	6.5	17	S = 90.80 mV·decade^{-1}
Ref. [133]	Lithium-based electrode and electrolyte	$Li_7La_3Zr_2O_{12}$-Au-Li_2CO_3	< 60	—	S = 56.43 mV·decade^{-1}
Ref. [102]	Lanthanum oxide-doped tin dioxide nanofibers	La_2O_3/SnO_2	—	—	R = 5.1
	Gold-lanthanum oxide-doped tin dioxide nanofibers	Au-La_2O_3/SnO_2	—	—	R = 10.1
Ref. [134]	Complex carbonate electrolyte with lithium titanate electrode	Li_2CO_3 + $CaCO_3$ with Li_2TiO_3	< 60	< 60	R = −0.05 V
Ref. [135]	Proton-conducting electrolytes	$La_{0.9}Sr_{0.1}YO_{3-\delta}$	1800	—	R = 1–10 μA·vol%$^{-1}$
Ref. [136]	Potassium chloride electrolyte with copper oxides electrode	Cu_xO/Cu	11.2	—	R = 0.016 A·ppm^{-1}
Ref. [82]	Palladium-perovskite oxides	Pd-$LaFeO_3$	—	—	R = 1
Ref. [137]	LCFO nanoparticles	$LaCo_{0.1}Fe_{0.9}O_3$	6	42	R = 6.69

catalytic properties, synergistic effect, and a big dielectric constant. The nanocomposite structure of $BaTiO_3$–CuO–Ag provides a large surface area for gas interactions, facilitating effective adsorption and desorption of CO_2 molecules. This enhancement in surface interactions can lead to increased sensitivity to CO_2 gas and improved sensor performance. By incorporating CuO and Ag nanoparticles into the $BaTiO_3$ matrix, the electrical conductivity of the nanocomposite is increased. This improvement facilitates quicker and more accurate detection of resistance changes induced by CO_2 gas. Joshi et al. [100] attributed the good performance and structural stability of this sensing material to the electrical and chemical contributions of Ag and CuO, which could create alternating nanointerfaces with $BaTiO_3$ spheres.

Both CuO and Ag nanoparticles have high catalytic properties, which can promote and facilitate the oxidation and reduction reactions involved in the sensing process. Ag increases the sensitivity of the sensing material by catalyzing the carbonation reaction, affecting the acceptor density and reducing the potential barrier between CuO and $BaTiO_3$ [100]. On the other hand, the combination of $BaTiO_3$, CuO, and Ag nanoparticles in the nanocomposite leads to a synergistic effect, whereby the individual properties of each component improve the performance of the sensing material. To support this claim, $BaTiO_3$ is highly sensitive to changes in the surrounding environment due to its big dielectric constant and ferroelectric properties. Therefore, by incorporating CuO and Ag nanoparticles into the nanocomposite, its sensing capabilities are further improved. Consequently, the catalytic effect, along with the combined effect, improves the sensitivity and stability of the sensor, promoting efficient detection of CO_2 gas. In addition to the $BaTiO_3$–CuO–Ag nanocomposite, Hsu et al. [102] reported a high response ratio (R = 10.1) for Au-La_2O_3-doped SnO_2 nanofibers compared to other sensing materials in CO_2-based sensors (Table 3). The presence of Au nanoparticles in the nanofibers facilitates efficient electron transfer between gas molecules and the sensing material. Such an electron transfer process increases the electrical conductivity of the nanofibers, which can improve the response ratio of the sensor to CO_2 gas. Hsu et al. [102] expressed that Au particles effectively improved the sensor response by 50%.

The research findings of several literature studies for CO_2-based sensors (Table 3) revealed that nanostructures, including nanocomposites, nanofilms, and nanofibers, had higher sensitivity and response ratio compared to those of conventional materials such as powders of barium carbonate ($BaCO_3$)-doped cobalt oxide (Co_3O_4) [103], La_2O_3/SnO_2 stacked layers [104], and thick films of lanthanum oxychloride (LaOCl)-doped SnO_2 [105]. In contrast to CH_4-based sensors, the performance of CO_2 gas sensors utilizing a designed ternary hybrid structure of sensing materials was better than that of the double hybrid structure, such as Sn-doped CdO [106] and LaOCl-doped SnO_2 [105]. Such improvement may be attributed to a combination of synergistic and catalytic effects. Both CuO and SnO_2 can serve as components of this ternary hybrid structure of sensing materials.

The data in Tables 1–3 indicate that metal oxides and metal catalysts are the most commonly used sensing materials in resistance-based sensors for detecting GHG. Fig. 7 illustrates the bubble cloud diagram of metal oxides and metal catalysts used in the studies reviewed for GHG detection. Based on the data in Table 1 and Fig. 7, SnO_2 metal oxide and Pd metal catalyst were the most frequently used materials for detecting CH_4 emissions, appearing in 43% and 17% of the reviewed studies, respectively. Additionally, SnO_2 was used in 36% and 26% of the reviewed studies, respectively, for the detection of N_2O and CO_2 emissions (Tables 2 and 3 and Fig. 7). In this regard, Love et al. [38] also reported the common use of tin oxide in their study. Following SnO_2, the metal oxides WO_3 and CuO were used in 21% and 20% of the studies reviewed, respectively, for detecting N_2O and CO_2 emissions in resistance-based sensors, as illustrated in Fig. 7. The data in Fig. 7 indicates that sensing technologies using nanostructured metal oxides and metal catalysts provide a more reliable and accurate measurement of GHG emissions compared to carbon nanotubes and polymers. In other words, metal oxides are used as high-potential materials for detecting a wide variety of GHGs due to their high sensitivity, fast response, very low cost, and user friendliness [138,139]. The strong performance of metal oxides can be attributed to their structural and morphological features. Metal oxides have a wide band gap, enabling a complete range of unique physical and chemical properties. Furthermore, many metal oxides and their compounds have catalytic abilities that can be highly effective in interacting with target gases [19].

3.4. Performance evaluation of different sensing mechanisms in CH_4-, N_2O-, and CO_2-based sensors and their limitations

Different users, including agricultural and environmental experts and farmers, can select the most suitable and effective sensing mechanisms for generating accurate data on GHG emissions by understanding the advantages and disadvantages of different sensing techniques. However, by generating accurate data, a more reliable understanding of GHG emissions and their impacts on the environment and crop production can be provided. Additionally, by applying the appropriate sensing mechanisms, we can ensure optimal and efficient resource use while minimizing the maintenance and operational costs of the sensor, which is one of the primary goals in precision agriculture.

The advantages and disadvantages of the sensing mechanisms are outlined in Table 4 [14,23–25,27,43,62,140–147]. The data of Table 4 is derived from the findings of the studies presented in Tables 1, 2, and 3. When analyzing GHG sensors, factors such as sensitivity or response ratio at low concentrations, real-time monitoring, cost effectiveness, and portability were considered as key components contributing to the advantages of the sensing mechanisms. By using effective sensor mechanisms, GHG emissions can be continuously monitored and detected with high speed and accuracy. This information can be used to develop a plan that safeguards animals or agricultural products from adverse effects. Conversely, the factors of initial cost, sensitivity to environmental influences, complexity and difficulty in interpreting data were considered significant disadvantages of the sensing mechanisms. Nevertheless, acknowledging these elements as disadvantages may require a considerable investment in the purchase, installation, calibration, and maintenance of sensors to obtain reliable readings of GHG.

However, after a closer look at the literature review on the performance of different sensing mechanisms, some limitations are revealed. Two known limiting variables in the RM-based mechanism are limited sensitivity and environmental effects such as temperature and humidity, which can reduce the accuracy of the GHG sensors [45]. When there is noise or interference, through the RM-based mechanisms, minor changes in resistance with low accuracy can be detected. The FET- and SAW-based mechanisms have a

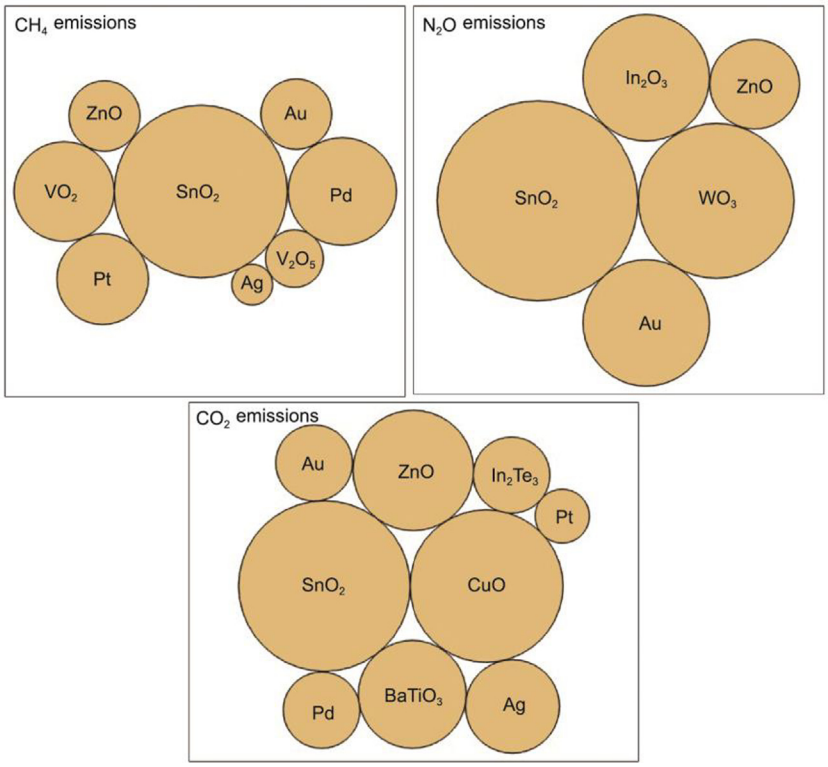

Fig. 7. Bubble cloud diagram of metal oxides and metal catalysts utilized in the studies reviewed in the detection of GHG. The different sizes of the bubbles reflect their increased usage.

Table 4
The advantages and disadvantages of the sensing mechanisms in CH_4-, N_2O-, and CO_2-based sensors.

Sensing mechanism	Advantage				Disadvantage			
	Sensitivity in low concentrations	Real-time monitoring	Cost-effective	Portable application	Sensitivity to environmental factors	Complexity	Hard interpretation of data	References
Resistance measurement	Moderate to high	*	—	—	*	—	—	[43,62]
Field effect transistor	Moderate	*	*	*	*	*	*	[24,25,140,141]
Surface acoustic wave	Moderate	*	*	*	*	*	*	[27,142]
Electrochemical	High	*	*	—	*	—	—	[23,143,144]
Catalytic	High	—	—	—	*	—	—	[14,145]
Chromatography	High	—	—	—	—	*	*	[23]
Optical	Moderate	*	—	*	*	*	*	[146,147]

The asterisk (*) symbol indicates that the sensing mechanism possesses the relevant feature.

restricted sensitivity range and may not be suitable for measuring very low or very high values of GHG emissions [140,141]. Working electrodes in sensors utilizing electrochemical mechanisms, as well as catalytic sensors, are often designed to respond to a specific target gas. Their effectiveness and selectivity may be compromised when other substances or environments with multiple potential interferents are detected [29]. This limitation can affect the accuracy of measurements in complex matrices. Additionally, electrochemical and catalytic sensors require regular maintenance and calibration over time due to chemical reactions taking place on the electrode's surface [55,65,95]. The gas chromatography technique is expensive and time-consuming, requiring skilled personnel for sample analysis and a complex process setup [32]. In optical sensors, signal degradation can occur due to interference, absorption, and scattering, particularly in complex media or turbid samples. These optical sensors should be regularly calibrated because of variations in the intensity of the light source and the length of the optical path [18,58]. Besides, the application of optical sensors is limited due to their high cost. According to recent research, resistance- and electrochemical-based sensors provide significant advantages for CO_2 and CH_4 detection due to their high sensitivity, simplicity, ease of use, and low cost in device fabrication [43,66,76,85,102]. However, several other sensing mechanisms, such as optical, chromatography, FET and SAW techniques, have not yet achieved a level of development that is high enough for N_2O detection.

3.5. Investigating the effect of environmental temperature and humidity on the performance of GHG sensors and offering strategies for different conditions

The GHG sensors can be used in various environmental conditions, from humid tropical climates to dry arid regions. In this context, changes in humidity and temperature can affect the sensors' readings, leading to inaccurate and unreliable measurements of GHG concentrations [45,148–150]. By investigating and comprehending the environmental impacts on sensor performance, researchers can be assisted to ensure reliability and stability when measuring GHG concentrations over time. Furthermore, by understanding the performance range of sensors based on humidity and temperature, appropriate sensors can be selected for specific environments and it can help to determine the frequency of maintenance and calibration.

Generally, the reactivity and electrical conductivity of various sensing materials, particularly metal oxide semiconductors, rise with an increase of operating temperature, which can affect their interaction with target gases and the sensor output signal, respectively [43]. In most cases, a rise in temperature leads to greater sensitivity and shorter response and recovery time for the sensor. Through such an increase in sensitivity in sensors, GHG in low concentrations can be detected. In contrast to temperature, high humidity may increase the response and recovery time of sensors, because water molecules compete with GHG molecules for adsorption on the surface of the sensor material [14]. This competition reduces the sensitivity of the sensor to target gases. Liu et al. [151] investigated the impact of temperature on CO_2 concentration measurements by the infrared sensor. Their findings revealed that gas concentration measurement values (level of detection) decreased concomitantly with the decline of temperature and humidity.

Researchers are trying to build and develop sensors with a flexible operating temperature and high humidity resistance to increase performance with minimal fluctuations [150]. Yuan et al. [150] noted that Ag_2Te nanowires were humidity-resistant, which could provide a new pathway for developing room-temperature humidity-resistant gas sensors. The results of the reviewed studies on CH_4 gas indicated that the Pd-SnO_2 with an operating temperature ranging from 25 (room temperature) [46] to 400 °C [50] had strong performance in terms of sensitivity, response ratio, response time, and recovery time. Regarding N_2O gas, sensing materials such as SnO_2-graphene nanomaterial [81], In_2O_3 nanowires [85], and WO_3 nanowires [85] had good performance in terms of response and recovery time at 25, 150, and 250 °C, respectively. $BaTiO_3$–CuO and $BaTiO_3$–CuO–Ag thin films, as studied by Herrán et al. [112] and Herrán et al. [101], respectively, had flexibility in operating temperatures ranging from 25 to 250 °C for CO_2 gas detection.

Long-term exposure to high temperatures and humidity can accelerate the degradation of sensing materials, reducing their lifespan and performance [152]. Fig. 8 highlights practical strategies in the effective use of GHG sensors for different environmental conditions. As illustrated in Fig. 8, regular calibration of sensors [153], the implementation of temperature and humidity compensation techniques [154], correct placement of sensors, provision of thermal insulation [155], effective sealing to prevent interference from humidity and other external factors [156], and consistently monitoring on sensors [157] are crucial strategies for optimizing the performance of GHG sensors under different environmental conditions.

4. Conclusions

By understanding the challenges in the performance of GHG sensors, constructive suggestions and solutions can be effectively provided to raise the detection level of GHG emissions. In this regard, by recognizing current challenges and providing constructive suggestions, farm management practices and strategies can be improved. The primary challenges in various studies include

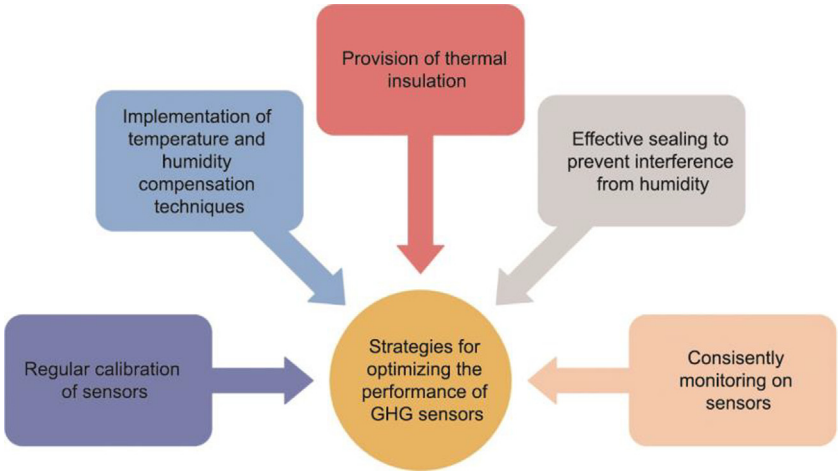

Fig. 8. Practical strategies in the effective use of GHG sensors for different environmental conditions.

detecting low concentrations of GHG in complex environments, distinguishing target gases from interfering substances, maintaining consistent performance over time and under different conditions, developing sensors, and minimizing energy requirements for practical applications. Therefore, potential solutions and constructive suggestions for increasing the accuracy and efficiency of GHG sensors can be sought through several key parts, including advanced materials and nanostructures, sensor design and optimization, calibration and validation, and cost reduction. In connection with advanced materials and nanostructures, the selection of materials featuring nanostructures with a big SSA and strong affinity for GHG, such as Pd-doped SnO_2 nanoparticles, In_2O_3 nanowires, WO_3 nanowires, and Au-La_2O_3-doped SnO_2 nanofibers, can be highly effective in the detection of GHG. From the perspective of sensor design, the development of hybrid sensors based on technology (such as optical, electrochemical, and thermal) and materials (double and triple hybrids) can significantly affect sensor optimization. Among other constructive suggestions, by using accurate and verifiable reference standards for GHG concentrations and doing comparative studies among different types of sensors, we can ensure the control process and data quality. Additionally, using low-power components and circuits to minimize energy consumption and costs, along with using wireless sensor networks for ongoing remote monitoring and data transmission, is essential. Finally, the accuracy and efficiency of GHG sensors in the agricultural sector can be improved by applying these constructive suggestions, leading to improved monitoring of gas emissions, reduced environmental impacts, and more sustainable agricultural practices.

Declaration of competing interest

The authors declare that they have no known competing financial interests or personal relationships that could have appeared to influence the work reported in this paper.

Acknowledgments

This work was supported by the National Natural Science Foundation of China (32271980) and the Key Pioneer Research Project of Zhejiang Province (2022C02014).

References

[1] Montzka SA, Dlugokencky EJ, Butler JH. Non-CO_2 greenhouse gases and climate change. Nature 2011;476(7358):43–50.
[2] Ansuategi A, Escapa M. Economic growth and greenhouse gas emissions. Ecol Econ 2002;40(1):23–37.
[3] Lamb WF, Wiedmann T, Pongratz J, Andrew R, Crippa M, Olivier JGJ, et al. A review of trends and drivers of greenhouse gas emissions by sector from 1990 to 2018. Environ Res Lett 2021;16(7):073005.
[4] Olivier JG, Schure K, Peters J. Trends in global CO_2 and total greenhouse gas emissions. Report. Hague: PBL Netherlands Environmental Assessment Agency 2020.
[5] Xuan X, Zhang F, Deng X, Bai Y. Measurement and spatio-temporal transfer of greenhouse gas emissions from agricultural sources in China: a food trade perspective. Resour Conserv Recycling 2023;197:107100.
[6] Wu Q, He Y, Qi Z, Jiang Q. Drainage in paddy systems maintains rice yield and reduces total greenhouse gas emissions on the global scale. J Clean Prod 2022;370:133515.
[7] Vaghar Seyedin SM, Zeidi A, Chamanehpour E, Nasri MH, Vargas-Bello-Pérez E. Methane emission: strategies to reduce global warming in relation to animal husbandry units with emphasis on ruminants. Sustainability 2022;14(24):16897.
[8] Petersen SO, Peixoto LEK, Sørensen H, Tariq A, Brændholt A, Hansen LV, et al. Higher N_2O emissions from organic compared to synthetic N fertilisers on sandy soils in a cool temperate climate. Agric Ecosyst Environ 2023;358:108718.
[9] He Z, Ding B, Pei S, Cao H, Liang J, Li Z. The impact of organic fertilizer replacement on greenhouse gas emissions and its influencing factors. Sci Total Environ 2023;905:166917.
[10] Galic M, Mesic M, Zgorelec Z. Influence of organic and mineral fertilization on soil greenhouse gas emissions. A review. ACS Agric Conspec Sci 2020;85:1–8.
[11] Avagyan AB. Theory of bioenergy accumulation and transformation: application to evolution, energy, sustainable development, climate change, manufacturing, agriculture, military activity and pandemic challenges. Athens J Sci 2021;8(1):57–80.
[12] Aslan MF, Durdu A, Sabanci K, Ropelewska E, Gültekin SS. A comprehensive survey of the recent studies with uav for precision agriculture in open fields and greenhouses. Appl Sci 2022;12(3):1047.
[13] Kim MY, Lee KH. Electrochemical sensors for sustainable precision agriculture—a review. Front Chem 2022;10:848320.
[14] Santhanam KSV, Ahamed NN. Greenhouse gas sensors fabricated with new materials for climatic usage: a review. ChemEngineering 2018;2(3):38.
[15] Borhan M, Khanaum M. Sensors and methods for measuring greenhouse gas emissions from different components of livestock production facilities. J Geosci Environ Prot 2022;10(12):242–72.
[16] Zaman M, Müller C, Chang S, Sanz-Cobena A. Measuring emission of agricultural greenhouse gases and developing mitigation options using nuclear and related techniques. Berlin: Springer Nature; 2021.
[17] Milam-Guerrero J, Yang B, To DT, Myung NV. Nitrous oxide is no laughing matter: a historical review of nitrous oxide gas-sensing capabilities highlighting the need for further exploration. ACS Sens 2022;7(12):3598–610.
[18] Liu X, Cheng S, Liu H, Hu S, Zhang D, Ning H. A survey on gas sensing technology. Sensors 2012;12(7):9635–65.
[19] Gautam YK, Sharma K, Tyagi S, Ambedkar AK, Chaudhary M, Pal SB. Nanostructured metal oxide semiconductor-based sensors for greenhouse gas detection: progress and challenges. R Soc Open Sci 2021;8(3):201324.
[20] Mulmi S, Thangadurai V. Editors' choice—review—solid-state electrochemical carbon dioxide sensors: fundamentals, materials and applications. J Electrochem Soc 2020;167(3):037567.
[21] Rajasekar P, Selvi JAV. Sensing and analysis of greenhouse gas emissions from rice fields to the near field atmosphere. Sensors 2022;22(11):4141.

[22] Majhi SM, Mirzaei A, Kim HW, Kim SS, Kim TW. Recent advances in energy-saving chemiresistive gas sensors: a review. Nano Energy 2021;79:105369.
[23] Aldhafeeri T, Tran MK, Vrolyk R, Pope M, Fowler M. A review of methane gas detection sensors: recent developments and future perspectives. Inventions 2020;5(3):28.
[24] Zhang P, Xiao Y, Zhang J, Liu B, Ma X, Wang Y. Highly sensitive gas sensing platforms based on field effect transistor—a review. Anal Chim Acta 2021;1172:338575.
[25] Bushra KA, Prasad KS. Based field-effect transistor sensors. Talanta 2022;239:123085.
[26] Zhang J, Liu L, Yang Y, Huang Q, Li D, Zeng D. A review on two-dimensional materials for chemiresistive- and FET-type gas sensors. Phys Chem Chem Phys 2021;23(29):15420–39.
[27] Kumar A, Prajesh R. The potential of acoustic wave devices for gas sensing applications. Sens Actuators A Phys 2022;339:113498.
[28] Morales-Rodriguez ME, Joshi PC, Humphries JR, Fuhr PL, Mcintyre TJ. Fabrication of low cost surface acoustic wave sensors using direct printing by aerosol inkjet. IEEE Access 2018;6:20907–15.
[29] Yunusa Z, Hamidon MN, Kaiser A, Awang Z. Gas sensors: a review. Sens Transducers 2014;168(4):61–75.
[30] Brauns E, Morsbach E, Kunz S, Bäumer M, Lang W. A fast and sensitive catalytic gas sensors for hydrogen detection based on stabilized nanoparticles as catalytic layer. Sens Actuators B Chem 2014;193:895–903.
[31] Lee JH, Park MS, Jung H, Choe YS, Kim W, Song YG, et al. Selective C_2H_2 detection with high sensitivity using SnO_2 nanorod based gas sensors integrated with a gas chromatography. Sens Actuators B Chem 2020;307:127598.
[32] Pascale R, Caivano M, Buchicchio A, Mancini IM, Bianco G, Caniani D. Validation of an analytical method for simultaneous high-precision measurements of greenhouse gas emissions from wastewater treatment plants using a gas chromatography-barrier discharge detector system. J Chromatogr A 2017;1480:62–9.
[33] Bogue R. Detecting gases with light: a review of optical gas sensor technologies. Sens Rev 2015;35(2):133–40.
[34] Li J, Yu Z, Du Z, Ji Y, Liu C. Standoff chemical detection using laser absorption spectroscopy: a review. Remote Sens 2020;12(17):2771.
[35] Xu M, Peng B, Zhu X, Guo Y. Multi-gas detection system based on non-dispersive infrared (NDIR) spectral technology. Sensors 2022;22(3):836.
[36] Yang T, Chen W, Wang P. A review of all-optical photoacoustic spectroscopy as a gas sensing method. Appl Spectrosc Rev 2021;56(2):143–70.
[37] Hoa ND, Duy NV, El-Safty SA, Hieu NV. Meso-/nanoporous semiconducting metal oxides for gas sensor applications. J Nanomater 2015;2015:972025.
[38] Love C, Nazemi H, El-Masri E, Ambrose K, Freund MS, Emadi A. A review on advanced sensing materials for agricultural gas sensors. Sensors 2021;21(10):3423.
[39] Yan Y, Yang G, Xu J, Zhang M, Kuo CC, Wang SD. Conducting polymer-inorganic nanocomposite-based gas sensors: a review. Sci Technol Adv Mater 2020;21(1):768–86.
[40] Park SJ, Park CS, Yoon H. Chemo-electrical gas sensors based on conducting polymer hybrids. Polymers 2017;9(5):155.
[41] Wang Y, Liu A, Han Y, Li T. Sensors based on conductive polymers and their composites: a review. Polym Int 2020;69(1):7–17.
[42] Kumari K, Ram S. Sensitivity study of nanocrystalline Fe_3BO_6 sensor for methane gas detection. IEEE Sens J 2018;18(20):8230–7.
[43] Abruzzi RC, Pires MJR, Dedavid BA, Galli CF. Application of SnO_2 nanoparticles and zeolites in coal mine methane sensors. Mater Res 2019;22(Suppl 1):e20180818.
[44] Yao L, Li Y, Ran Y, Yang Y, Zhao R, Su L, et al. Construction of novel Pd–SnO_2 composite nanoporous structure as a high-response sensor for methane gas. J Alloys Compd 2020;826:154063.
[45] Kooti M, Keshtkar S, Askarieh M, Rashidi A. Progress toward a novel methane gas sensor based on SnO_2 nanorods–nanoporous graphene hybrid. Sens Actuators B Chem 2019;281:96–106.
[46] Nasresfahani S, Sheikhi MH, Tohidi M, Zarifkar A. Methane gas sensing properties of Pd-doped SnO_2/reduced graphene oxide synthesized by a facile hydrothermal route. Mater Res Bull 2017;89:161–9.
[47] Chen R, Wang J, Luo S, Xiang L, Li W, Xie D. Unraveling photoexcited electron transfer pathway of oxygen vacancy-enriched ZnO/Pd hybrid toward visible light-enhanced methane detection at a relatively low temperature. Appl Catal B 2020;264:118554.
[48] Liang J, Li W, Liu J, Hu M. Room temperature CH_4 sensing properties of Au decorated VO_2 nanosheets. Mater Lett 2016;184:92–5.
[49] Lančok J, Santoni A, Penza M, Loreti S, Menicucci I, Minarini C, et al. Tin oxide thin films prepared by laser-assisted metal-organic CVD: structural and gas sensing properties. Surf Coat Tech 2005;200(1–4):1057–60.
[50] Wagner T, Bauer M, Sauerwald T, Kohl CD, Tiemann M. X-ray absorption near-edge spectroscopy investigation of the oxidation state of Pd species in nanoporous SnO_2 gas sensors for methane detection. Thin Solid Films 2011;520(3):909–12.
[51] Wu Z, Chen X, Zhu S, Zhou Z, Yao Y, Quan W, et al. Room temperature methane sensor based on graphene nanosheets/polyaniline nanocomposite thin film. IEEE Sens J 2012;13(2):777–82.
[52] Fu J, Zhao C, Zhang J, Peng Y, Xie E. Enhanced gas sensing performance of electrospun Pt-functionalized NiO nanotubes with chemical and electronic sensitization. ACS Appl Mater Interfaces 2013;5(15):7410–6.
[53] Prasad AK, Amirthapandian S, Dhara S, Dash S, Murali N, Tyagi AK. Novel single phase vanadium dioxide nanostructured films for methane sensing near room temperature. Sens Actuators B Chem 2014;191:252–6.
[54] Vuong NM, Hieu NM, Hieu HN, Yi H, Kim D, Han YS, et al. Ni_2O_3-decorated SnO_2 particulate films for methane gas sensors. Sens Actuators B Chem 2014;192:327–33.
[55] Wang Z, Guo M, Baker GA, Stetter JR, Lin L, Mason AJ, et al. Methane–oxygen electrochemical coupling in an ionic liquid: a robust sensor for simultaneous quantification. Analyst 2014;139(20):5140–7.
[56] Amutha A, Amirthapandian S, Prasad A, Panigrahi B, Thangadurai P. Methane gas sensing at relatively low operating temperature by hydrothermally prepared SnO_2 nanorods. J Nanopart Res 2015;17(7):289.
[57] Karami Horastani Z, Sayedi SM, Sheikhi MH, Rahimi E. Effect of silver additive on electrical conductivity and methane sensitivity of SnO_2. Mater Sci Semicond Process 2015;35:38–44.
[58] Yang J, Zhou L, Huang J, Tao C, Li X, Chen W. Sensitivity enhancing of transition mode long-period fiber grating as methane sensor using high refractive index polycarbonate/cryptophane A overlay deposition. Sens Actuators B Chem 2015;207:477–80.
[59] Li W, Liang J, Liu J, Zhou L, Yang R, Hu M. Synthesis and room temperature CH_4 gas sensing properties of vanadium dioxide nanorods. Mater Lett 2016;173:199–202.
[60] Liang J, Liu J, Li N, Li W. Magnetron sputtered Au-decorated vanadium oxides composite thin films for methane-sensing properties at room temperature. J Alloys Compd 2016;671:283–90.
[61] Liang J, Liu J, Li W, Hu M. Preparation and room temperature methane sensing properties of platinum-decorated vanadium oxide films. Mater Res Bull 2016;84:332–9.
[62] Dhivya P, Prasad AK, Sridharan M. Nanostructured perovskite $CdTiO_3$ films for methane sensing. Sens Actuators B Chem 2016;222:987–93.
[63] Schneider K, Lubecka M, Czapla A. V_2O_5 thin films for gas sensor applications. Sens Actuators B Chem 2016;236:970–7.
[64] Shaalan N, Rashad M, Moharram A, Abdel-Rahim M. Promising methane gas sensor synthesized by microwave-assisted Co_3O_4 nanoparticles. Mater Sci Semicond Process 2016;46:1–5.
[65] Yin H, Wan H, Lin L, Zeng X, Mason AJ. Miniaturized planar RTIL-based eletrochemical gas sensor for real-time point-of-exposure monitoring. In: Proceedings of 2016 IEEE Healthcare Innovation Point-of-Care Technologies Conference (HI-POCT); 2016 Nov 9–11; Cancun, Mexico. Piscataway: IEEE; 2016. p. 85–8.
[66] Sekhar PK, Kysar J, Brosha EL, Kreller CR. Development and testing of an electrochemical methane sensor. Sens Actuators B Chem 2016;228:162–7.
[67] Fedorenko G, Oleksenko L, Maksymovych N, Skolyar G, Ripko O. Semiconductor gas sensors based on Pd/SnO_2 nanomaterials for methane detection in air. Nanoscale Res Lett 2017;12:329.
[68] Oleksenko L, Fedorenko G, Maksymovych N. Platinum-containing adsorption-semiconductor sensors based on nanosized tin dioxide for methane detection. Theor Exp Chem 2017;53(4):259–64.
[69] Chimowa G, Tshabalala ZP, Akande AA, Bepete G, Mwakikunga B, Ray SS, et al. Improving methane gas sensing properties of multi-walled carbon nanotubes by vanadium oxide filling. Sens Actuators B Chem 2017;247:11–8.
[70] Yang L, Wang Z, Zhou X, Wu X, Han N, Chen Y. Synthesis of Pd-loaded mesoporous SnO_2 hollow spheres for highly sensitive and stable methane gas sensors. RSC Advance 2018;8(43):24268–75.
[71] Aghagoli Z, Ardyanian M. Synthesis and study of the structure, magnetic, optical and methane gas sensing properties of cobalt doped zinc oxide microstructures. J Mater Sci Mater Electron 2018;29(9):7130–41.
[72] Lu W, Ding D, Xue Q, Du Y, Xiong Y, Zhang J, et al. Great enhancement of CH_4 sensitivity of SnO_2 based nanofibers by heterogeneous sensitization and catalytic effect. Sens Actuators B Chem 2018;254:393–401.
[73] Zhang D, Wu Z, Li P, Zong X, Dong G, Zhang Y. Facile fabrication of polyaniline/multi-walled carbon nanotubes/molybdenum disulfide ternary nanocomposite and its high-performance ammonia-sensing at room temperature. Sens Actuators B Chem 2018;258:895–905.
[74] Dosi M, Lau I, Zhuang Y, Simakov DS, Fowler MW, Pope MA. Ultrasensitive electrochemical methane sensors based on solid polymer electrolyte-infused laser-induced graphene. ACS Appl Mater Interfaces 2019;11(6):6166–73.
[75] Zhang S, Li Y, Sun G, Zhang B, Wang Y, Cao J, et al. Enhanced methane sensing properties of porous NiO nanaosheets by decorating with SnO_2. Sens Actuators B Chem 2019;288:373–82.
[76] Hong P, Li Y, Zhang X, Peng S, Zhao R, Yang Y, et al. Nanoporous network SnO_2 constructed with ultra-small nanoparticles for methane gas sensor. J Mater Sci Mater Electron 2019;30(15):14325–34.
[77] Xue D, Wang P, Zhang Z, Wang Y. Enhanced methane sensing property of flower-like SnO_2 doped by Pt nanoparticles: a combined experimental and first-principle study. Sens Actuators B Chem 2019;296:126710.
[78] Yang B, Xu J, Wang C, Xiao J. A potentiometric sensor based on $SmMn_2O_5$ sensing electrode for methane detection. Mater Chem Phys 2020;245:122679.
[79] Li X, Li Y, Sun G, Zhang B, Wang Y, Zhang Z. Enhanced CH_4 sensitivity of porous nanosheets-assembled ZnO microflower by decoration with Zn_2SnO_4. Sens Actuators B Chem 2020;304:127374.
[80] Mounasamy V, Mani GK, Ponnusamy D, Tsuchiya K, Reshma P, Prasad AK, et al. Investigation on CH_4 sensing characteristics of hierarchical V_2O_5 nanoflowers operated at relatively low temperature using chemiresistive approach. Anal Chim Acta 2020;1106:148–60.

[81] Fu H, Wang X, Ding J, Yan X, Zhao Z, Zhang Z. SnO_2/Graphene incorporated optical fiber Mach–Zehnder interferometer for methane gas detection. Opt Fiber Technol 2022;74:103126.
[82] Li J, Ma Y, Duan Z, Zhang Y, Duan X, Liu B, et al. Local dynamic neural network for quantitative analysis of mixed gases. Sens Actuators B Chem 2024;404:135230.
[83] Shi J, Jiang Y, Duan Z, Li J, Yuan Z, Tai H. Designing an optical gas chamber with stepped structure for non-dispersive infrared methane gas sensor. Sens Actuators A Phys 2024;367:115052.
[84] Deb B, Desai S, Sumanasekera GU, Sunkara MK. Gas sensing behaviour of mat-like networked tungsten oxide nanowire thin films. Nanotechnology 2007;18 (28):285501.
[85] Rout CS, Ganesh K, Govindaraj A, Rao CNR. Sensors for the nitrogen oxides, NO_2, NO and N_2O, based on In_2O_3 and WO_3 nanowires. Appl Phys A Mater Sci Process 2006;85(3):241–6.
[86] Polleux J, Gurlo A, Barsan N, Weimar U, Antonietti M, Niederberger M. Template-free synthesis and assembly of single-crystalline tungsten oxide nanowires and their gas-sensing properties. Angew Chem Int Ed 2005;45 (2):261–5.
[87] Chung YK, Kim MH, Um WS, Lee HS, Song JK, Choi SC, et al. Gas sensing properties of WO_3 thick film for NO_2 gas dependent on process condition. Sens Actuators B Chem 1999;60(1):49–56.
[88] Cantalini C, Sun HT, Faccio M, Pelino M, Santucci S, Lozzi L, et al. NO_2 sensitivity of WO_3 thin film obtained by high vacuum thermal evaporation. Sens Actuators B Chem 1996;31(1–2):81–7.
[89] Chaturvedi A, Mishra VN, Dwivedi R, Srivastava SK. Selectivity and sensitivity studies on plasma treated thick film tin oxide gas sensors. Microelectronics J 2000;31(4):283–90.
[90] Kanazawa E, Kugishima M, Shimanoe K, Kanmura Y, Teraoka Y, Miura N, et al. Mixed-potential type N_2O sensor using stabilized zirconia- and SnO_2-based sensing electrode. Sens Actuators B Chem 2001;75(1–2):121–4.
[91] Kanazawa E, Sakai G, Shimanoe K, Kanmura Y, Teraoka Y, Miura N, et al. Metal oxide semiconductor N_2O sensor for medical use. Sens Actuators B Chem 2001;77(1–2):72–7.
[92] Mukherjee K, Majumder SB. Reducing gas sensing behavior of nano-crystalline magnesium–zinc ferrite powders. Talanta 2010;81(4–5):1826–32.
[93] Asmah MT, Sidek O, Hutagalung SD. Junctionless silicon-based device for CO_2 and N_2O gas detection at room temperature. Procedia Manuf 2015;2:385–91.
[94] Kalyakin A, Volkov A, Demin A, Gorbova E, Tsiakaras P. Determination of nitrous oxide concentration using a solid-electrolyte amperometric sensor. Sens Actuators B Chem 2019;297:126750.
[95] Damgaard LR, Kelly C, Casciotti K, Ward BB, Revsbech NP. Amperometric sensor for nanomolar nitrous oxide analysis. Anal Chim Acta 2020;1101:135–40.
[96] Ramu AG, Umar A, Gopi S, Algadi H, Albargi H, Ibrahim AA, et al. Tetracyanonickelate (II)/KOH/reduced graphene oxide fabricated carbon felt for mediated electron transfer type electrochemical sensor for efficient detection of N_2O gas at room temperature. Environ Res 2021;201:111591.
[97] Silambarasan P, Moon IS. Enhancing the mediated electrochemical reduction process combined with developed liquid–gas electrochemical flow sensors for sustainable N_2O removal at room temperature. Environ Res 2022;204:111912.
[98] Rahman MT, Khan RR, Tian Y, Ibrahim H, Dong L. High-sensitivity and room-temperature nitrous oxide sensor using Au nanoparticles-decorated MoS_2. IEEE Sens J 2023;23(17):18994–9001.
[99] Turlybekuly A, Sarsembina M, Mentbayeva A, Bakenov Z, Soltabayev B. CuO/TiO_2 heterostructure-based sensors for conductometric NO_2 and N_2O gas detection at room temperature. Sens Actuators B Chem 2023;397:134635.
[100] Joshi S, Ippolito SJ, Periasamy S, Sabri YM, Sunkara MV. Efficient heterostructures of Ag@CuO/$BaTiO_3$ for low-temperature CO_2 gas detection: assessing the role of nanointerfaces during sensing by operando DRIFTS technique. ACS Appl Mater Interfaces 2017;9(32):27014–26.
[101] Herrán J, Mandayo GG, Ayerdi I, Castaño E. Influence of silver as an additive on $BaTiO_3$–CuO thin film for CO_2 monitoring. Sens Actuators B Chem 2008;129(1):386–90.
[102] Hsu KC, Fang TH, Hsiao YJ, Chan CA. Highly response CO_2 gas sensor based on Au-La_2O_3 doped SnO_2 nanofibers. Mater Lett 2020;261:127144.
[103] Kim DY, Kang H, Choi NJ, Park KH, Lee HK. A carbon dioxide gas sensor based on cobalt oxide containing barium carbonate. Sens Actuators B Chem 2017;248:987–92.
[104] Iwata T, Matsuda K, Takahashi K, Sawada K. CO_2 sensing characteristics of a La_2O_3/SnO_2 stacked structure with micromachined hotplates. Sensors 2017;17(9):2156.
[105] Trung DD, Toan LD, Hong HS, Lam TD, Trung T, Van Hieu N. Selective detection of carbon dioxide using LaOCl-functionalized SnO_2 nanowires for air-quality monitoring. Talanta 2012;88:152–9.
[106] Rajesh N, Kannan JC, Krishnakumar T, Bonavita A, Leonardi S, Neri G. Microwave irradiated Sn-substituted CdO nanostructures for enhanced CO_2 sensing. Ceram Int 2015;41(10):14766–72.
[107] Kim DH, Yoon JY, Park HC, Kim KH. CO_2-sensing characteristics of SnO_2 thick film by coating lanthanum oxide. Sens Actuators B Chem 2000;62(1):61–6.
[108] Marsal A, Dezanneau G, Cornet A, Morante JR. A new CO_2 gas sensing material. Sens Actuators B Chem 2003;95(1–3):266–70.
[109] Desai RR, Lakshminarayana D, Patel PB, Panchal CJ. Indium sesquitelluride (In_2Te_3) thin film gas sensor for detection of carbon dioxide. Sens Actuators B Chem 2005;107(2):523–7.
[110] Zhu Q, Qiu F, Quan Y, Sun Y, Liu S, Zou Z. Solid-electrolyte NASICON thick film CO_2 sensor prepared on small-volume ceramic tube substrate. Mater Chem Phys 2005;91(2–3):338–42.
[111] Herrán J, Mandayo GG, Castaño E. Physical behaviour of $BaTiO_3$–CuO thin-film under carbon dioxide atmospheres. Sens Actuators B Chem 2007;127 (2):370–5.
[112] Herrán J, Fernández-González O, Castro-Hurtado I, Romero T, Mandayo G, Castaño E. Photoactivated solid-state gas sensor for carbon dioxide detection at room temperature. Sens Actuators B Chem 2010;149(2): 368–72.
[113] Kim MY, Choi YN, Bae JM, Oh TS. Carbon dioxide sensitivity of La-doped thick film tin oxide gas sensor. Ceram Int 2012;38(Suppl 1):S657–60.
[114] Shim HB, Kang JH, Choi JW, Yoo KS. Characteristics of thick-film CO_2 sensors based on NASICON with Na_2CO_3–$CaCO_3$ auxiliary phases. J Electroceram 2006;17(2–4):971–4.
[115] Matheswaran P, Sathyamoorthy R, Asokan K. Effect of 130 MeV Au ion irradiation on CO_2 gas sensing properties of In_2Te_3 thin films. Sens Actuators B Chem 2013;177:8–13.
[116] Van Hieu N, Khoang ND, Trung DD, Toan LD, Van Duy N, Hoa ND. Comparative study on CO_2 and CO sensing performance of LaOCl-coated ZnO nanowires. J Hazard Mater 2013;244:209–16.
[117] Zhu Y, Thangadurai V, Weppner W. Garnet-like solid state electrolyte $Li_6BaLa_2Ta_2O_{12}$ based potentiometric CO_2 gas sensor. Sens Actuators B Chem 2013;176:284–9.
[118] Wang X, Qin H, Sun L, Hu J. CO_2 sensing properties and mechanism of nanocrystalline $LaFeO_3$ sensor. Sens Actuators B Chem 2013;188:965–71.
[119] Kannan PK, Saraswathi R, Rayappan JBB. CO_2 gas sensing properties of DC reactive magnetron sputtered ZnO thin film. Ceram Int 2014;40 (8):13115–22.
[120] Xiong Y, Zhang G, Zhang S, Zeng D, Xie C. Tin oxide thick film by doping rare earth for detecting traces of CO_2: operating in oxygen-free atmosphere. Mater Res Bull 2014;52:56–64.
[121] Habib M, Hussain SS, Riaz S, Naseem S. Preparation and characterization of ZnO nanowires and their applications in CO_2 gas sensors. Mater Today Proc 2015;2(10):5714–9.
[122] Dhahri R, Hjiri M, El Mir L, Fazio E, Neri F, Barreca F, et al. ZnO: Ca nanopowders with enhanced CO_2 sensing properties. J Phys D Appl Phys 2015;48(25):255503.
[123] Karaduman I, Demir M, Yıldız DE, Acar S. CO_2 gas detection properties of a TiO_2/Al_2O_3 heterostructure under UV light irradiation. Phys Scr 2015;90 (5):055802.
[124] Mardare D, Cornei N, Mita C, Florea D, Stancu A, Tiron V, et al. Low temperature TiO_2 based gas sensors for CO_2. Ceram Int 2016;42(6):7353–9.
[125] Ehsani M, Hamidon MN, Toudeshki A, Abadi MHS, Rezaeian S. CO_2 gas sensing properties of screen-printed La_2O_3/SnO_2 thick film. IEEE Sens J 2016;16(18):6839–45.
[126] Abdelmounaïm C, Amara Z, Maha A, Mustapha D. Effects of molarity on structural, optical, morphological and CO_2 gas sensing properties of nanostructured copper oxide films deposited by spray pyrolysis. Mater Sci Semicond Process 2016;43:214–21.
[127] Zhang W, Xie C, Zhang G, Zhang J, Zhang S, Zeng D. Porous $LaFeO_3$/SnO_2 nanocomposite film for CO_2 detection with high sensitivity. Mater Chem Phys 2017;186:228–36.
[128] Joshi S, Kumar CBR, Jones LA, Mayes ELH, Ippolito SJ, Sunkara MV. Modulating interleaved ZnO assembly with CuO nanoleaves for multifunctional performance: perdurable CO_2 gas sensor and visible light catalyst. Inorg Chem Front 2017;4(11):1848–61.
[129] Hien HT, Giang HT, Hieu NV, Trung T, Tuan CV. Elaboration of Pd-nanoparticle decorated polyaniline films for room temperature NH_3 gas sensors. Sens Actuators B Chem 2017;249:348–56.
[130] Lee J, Choi NJ, Lee HK, Kim J, Lim SY, Kwon JY, et al. Low power consumption solid electrochemical-type micro CO_2 gas sensor. Sens Actuators B Chem 2017;248:957–60.
[131] Tanvir NB, Yurchenko O, Laubender E, Pohle R, Sicard OV, Urban G. Zinc peroxide combustion promoter in preparation of CuO layers for conductometric CO_2 sensing. Sens Actuators B Chem 2018;257:1027–34.
[132] Zhang M, Chen H, Wang H. Improved sensing properties of CO_2 gas sensor based on Li_3PO_4–Li_2SiO_3 thin film compared with Li_3PO_4. J Electrochem Soc 2018;165(5):B167–73.
[133] Struzik M, Garbayo I, Pfenninger R, Rupp JLM. A simple and fast electrochemical CO_2 sensor based on $Li_7La_3Zr_2O_{12}$ for environmental monitoring. Adv Mater 2018;30(44):1804098.
[134] Ambekar P, Randhawa J. Surface conductivity of binary carbonate as a performance-governing parameter of an electrochemical CO_2 gas sensor. Bull Mater Sci 2021;44(3):235.
[135] Kalyakin AS, Medvedev DA, Volkov AN. Electrochemical sensors based on proton-conducting electrolytes for determination of concentration and diffusion coefficient of CO_2 in inert gases. Chem Eng Sci 2021;229:116046.
[136] Digvijay B, Amala J, Aravind S, Bhuvaneshwari S, Mohanraj P. Cu_xO/Cu based electrochemical sensor for the detection of CO_2 gas. Indian Chem Eng 2022;64(5):479–93.
[137] Duan X, Jiang Y, Liu B, Duan Z, Zhang Y, Yuan Z, et al. Enhancing the carbon dioxide sensing performance of $LaFeO_3$ by Co doping. Sens Actuators B Chem 2024;402:135136.

[138] Wetchakun K, Samerjai T, Tamaekong N, Liewhiran C, Siriwong C, Kruefu V, et al. Semiconducting metal oxides as sensors for environmentally hazardous gases. Sens Actuators B Chem 2011;160(1):580–91.
[139] Choi JK, Hwang IS, Kim SJ, Park JS, Park SS, Jeong U, et al. Design of selective gas sensors using electrospun Pd-doped SnO_2 hollow nanofibers. Sens Actuators B Chem 2010;150(1):191–9.
[140] Liu J, Cai H, Chen S, Pi J, Zhao L. A review on soil nitrogen sensing technologies: challenges, progress and perspectives. Agriculture 2023;13(4):743.
[141] Burton L, Jayachandran K, Bhansali S. The "real-time" revolution for *in situ* soil nutrient sensing. J Electrochem Soc 2020;167(3):037569.
[142] Cicek A, Arslan Y, Trak D, Okay FC, Kaya OA, Korozlu N, et al. Gas sensing through evanescent coupling of spoof surface acoustic waves. Sens Actuators B Chem 2019;288:259–65.
[143] Kuberský P, Navrátil J, Syrový T, Sedlák P, Nešpůrek S, Hamáček A. An electrochemical amperometric ethylene sensor with solid polymer electrolyte based on ionic liquid. Sensors 2021;21(3):711.
[144] Aghamalyan MA. Investigation of carbon dioxide interaction with transition metal dichalcogenides by first principles. J Contemp Phys 2022;57(2):166–9.
[145] Bíró F, Dücső C, Radnóczi GZ, Baji Z, Takács M, Bársony I. ALD nano-catalyst for micro-calorimetric detection of hydrocarbons. Sens Actuators B Chem 2017;247:617–25.
[146] Tabassum R, Kant R. Recent trends in surface plasmon resonance based fiber–optic gas sensors utilizing metal oxides and carbon nanomaterials as functional entities. Sens Actuators B Chem 2020;310:127813.
[147] Clarke JS, Achterberg EP, Connelly DP, Schuster U, Mowlem M. Developments in marine pCO_2 measurement technology; towards sustained *in situ* observations. TrAC Trends Anal Chem 2017;88:53–61.
[148] Abdullah AN, Kamarudin K, Mamduh SM, Adom AH, Juffry ZHM. Effect of environmental temperature and humidity on different metal oxide gas sensors at various gas concentration levels. IOP Conf Series Mater Sci Eng 2020;864(1):012152.
[149] Wei P, Ning Z, Ye S, Sun L, Yang F, Wong KC, et al. Impact analysis of temperature and humidity conditions on electrochemical sensor response in ambient air quality monitoring. Sensors 2018;182(2):59.
[150] Yuan Z, Zhao Q, Duan Z, Xie C, Duan X, Li S, et al. Ag_2Te nanowires for humidity-resistant trace-level NO_2 detection at room temperature. Sens Actuators B Chem 2022;363:131790.
[151] Liu Y, Ni X, Wu Y, Zhang W. Study on effect of temperature and humidity on the CO_2 concentration measurement. IOP Conf Ser Earth Environ Sci 2017;81:012083.
[152] Hooshmand S, Kassanos P, Keshavarz M, Duru P, Kayalan CI, Kale İ, et al. Wearable nano-based gas sensors for environmental monitoring and encountered challenges in optimization. Sensors 2023;23(20):8648.
[153] Furst L, Feliciano M, Frare L, Igrejas G. A portable device for methane measurement using a low-cost semiconductor sensor: development, calibration and environmental applications. Sensors 2021;21(22):7456.
[154] Akhter F, Alahi MEE, Siddiquei HR, Gooneratne CP, Mukhopadhyay SC. Graphene oxide (GO) coated impedimetric gas sensor for selective detection of carbon dioxide (CO_2) with temperature and humidity compensation. IEEE Sens J 2021;21(4):4241–9.
[155] Nagy Z, Rossi D, Hersberger C, Irigoyen SD, Miller C, Schlueter A. Balancing envelope and heating system parameters for zero emissions retrofit using building sensor data. Appl Energy 2014;131:56–66.
[156] Gagnon S, L'Hérault E, Lemay M, Allard M. New low-cost automated system of closed chambers to measure greenhouse gas emissions from the tundra. Agric Meteorol 2016;228:29–41.
[157] Liao SH, Tsai ST, Hsia WL. Controlling and monitoring greenhouse gas emissions using CPS and GHG sensors. In: Proceedings of 2023 IEEE 3rd International Conference on Electronic Communications, Internet of Things and Big Data (ICEIB); 2023 Apr 14–16; Taichung, China. Piscataway: IEEE; 2023. p. 68–70.